Growth of nanoparticles in dynamic plasma

V. Vekselman* and Y. Raitses
Princeton Plasma Physics Laboratory, Princeton, New Jersey 08540, USA

M. N. Shneider
Department of Mechanical and Aerospace Engineering, Princeton University, Princeton, New Jersey 08540, USA

(Received 12 October 2018; revised manuscript received 27 February 2019; published 20 June 2019)

Coagulation growth kinetics of nanoparticles in plasma is affected by interparticle electrostatic forces due to the charging phenomenon. In stationary plasmas, unipolar charging of particles results in retardation of particle growth and may result in a limitation on particle size. We demonstrate the opposite effect of enhanced particle growth in atmospheric pressure nonstationary arc discharge. Modeling of the nanoparticle growth kinetics reveals the formation of a bipolar charge distribution. As a result, reversed (attractive) Coulomb forces promote the formation of micrometer-size particles in a millisecond timescale as observed in experiment.

DOI: 10.1103/PhysRevE.99.063205

I. INTRODUCTION

In many different fields of nanoscale science, knowledge of the pathway by which particles are formed is critical. In plasmas, both intentional and unintentional production of nanoscale and microscale particles are commonly observed in laboratory experiments and industrial applications. These particles surrounded by a stationary plasma are subjected to charging processes resulting in the formation of a unipolar charge distribution as predicted by theory. As a result, Coulomb repulsion forces inhibit growth rate and limit the size of particles forming in plasma. This is observed as the formation of ordered structures in plasma [1] characterized by topological order. However, numerous dusty plasma studies reported about the formation of large agglomerated particles, thus questioning the validity of theory predictions. In an attempt to explain this contradiction, models predicting attraction between similarly charges macroparticles were proposed [2]. It was also proposed that the particles in plasma have opposite charges [3] and multigroup-size distribution [4]. A number of physical mechanisms which could potentially explain the formation of specific size and charge distributions of dusty particles were suggested, including the electron emission from these particles (secondary, thermionic, photoelectric, etc.) [3,5,6], charge fluctuations [7], effects of imaginary potential [8], and ion trapping [9]. The applicability of the orbit-motion-limited (OML) theory [10] for the description of dust-plasma interactions was addressed in Ref. [11], which developed the modified OML theory. The latter includes a more accurate description of particle charging and heat exchange processes. However, most of these models are lacking experimental validation and verification. In this work we demonstrate a fast (submillisecond) formation of micron-scale particles in a nearly thermal plasma generated by the atmospheric pressure arc discharge and propose their growth mechanism based on bipolar charging of particles. It is shown that the charging polarity of nanoparticles depends on their size.

II. SETUP

The arc geometry and operating conditions are described in Ref. [12]. The arc is formed between two graphite electrodes at subatmospheric pressure (66.7 kPa) of helium (Fig. 1). In the arc core, the plasma temperature T_{arc} is about 8000 K and the carbon ablated from electrodes is presumably in a gas phase [12]. A computational fluid dynamic (CFD) code has been used to extend measured plasma parameters and gas temperature into the arc periphery region (at radial distances greater than or equal to 5 mm from the arc core) (see Fig. 2); these CFD simulations (in ANSYS) were benchmarked with available experimental data [13]. Lower temperature at the arc periphery promotes the condensation of carbon vapor and the formation of nanoparticles [14]. These conditions for nanoparticle formation are different from ones used in typical nonequilibrium dusty plasmas, which are usually operated at lower pressure (hundreds of pascals) [15].

III. EXPERIMENT

To monitor these particles, we used a narrow-band fast frame imaging to record the whole growth process. To enhance the camera sensitivity and time resolution, a cw laser was used for backlighting. The source laser beam was shaped into a wide aperture collimated beam to ensure complete illumination of particles. A signal-to-noise ratio was further improved via suppression of plasma and electrode radiation by a narrow bandpass filter centered at the laser wavelength (632 nm). A set of frames showing formation of micron-scale particles is presented in Fig. 3 (see the Supplemental Material [16] for the complete video file). Only the bottom part of the electrodes is captured by the camera. An uneven background is formed by laser fringes. The top surface of the anode can be

*vekselman@pppl.gov

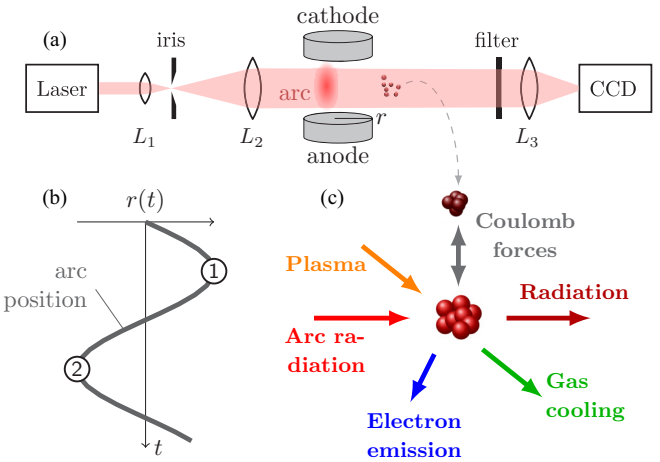

FIG. 1. Schematic of (a) the experimental setup, (b) arc motion, and (c) particle interactions.

partially observed in the images with a noticeable difference in the radiation intensity. The region of the highest intensity is associated with the arc attachment to the anode [17]. Thus, the arc is initially closer to the bottom edge of electrodes [0 μs, Fig. 3(a)] than in 660 μs [Fig. 3(b)], which corresponds to arc locations ① and ② in Fig. 1. This reflects a typical behavior of arcs demonstrating sporadic motion within an interelectrode gap [18].

The most interesting feature captured at 660 μs [Fig. 3(b)] is the presence of large micron-scale particles. Apparently, they are formed from the gas phase and smaller-size particles as evidenced by a short time interval of 16.5 μs between recorded frames (skipped in Fig. 3). Note that no particles were detected when the arc was away from the bottom edge of the electrodes. This observation implies a direct correlation between the proximity of the arc to the particle growth region and the formation of particles. The latter occurs at a submillisecond timescale, which is much shorter than the growth time typical for low-pressure dusty plasmas (on the order

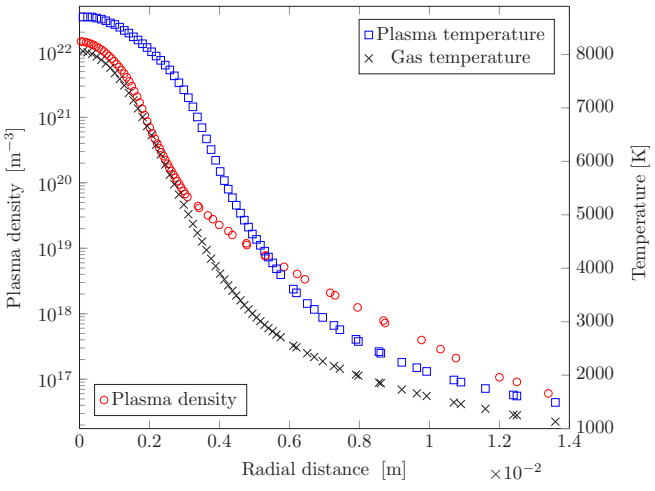

FIG. 2. Radial distribution of plasma density and temperature, and gas temperature in the arc. Profiles are calculated using ANSYS CFX code.

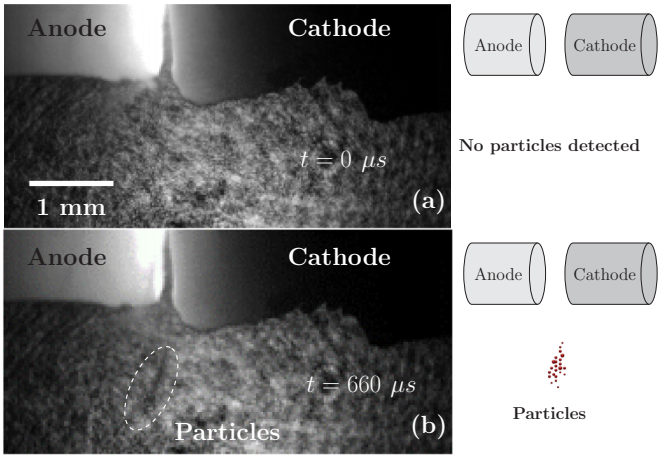

FIG. 3. Two selected frames (with 660-μs delay) recorded during the arc at 60 000 frames/s. The video resolution is 22 μm pixel^{-1} and the frame exposure time 5 μs. Particles of micron scale are encircled in (b) and schematically shown in the cartoon on the right.

of milliseconds) [8]. From these observations, we derive the following: The observed growth of particles occurs in a nonstationary plasma environment, no external influx of particles contributes to the growth, and Coulomb repulsion between particles is suppressed, allowing the growth of particles to micrometer-scale size.

In support of the above points, we propose the following explanation of the particle growth outside the arc which is complemented by the growth model described below. In the carbon arc, the electrode material is ablated and further evaporated in the hot arc core. Carbon vapor condenses in a colder plasma region (arc periphery) promoting the formation of nanoparticles. For nanoparticles less than a few nanometers in diameter, models of charge fluctuations [7] and image potential [8] describe well the process of the particle formation by coagulation in gas phase. However, larger nanoparticles are less sensitive to charge fluctuations due to accumulation of negative charge in plasma. As a result, in a steady state, the Coulomb repulsion may limit the growth of larger particles. In experiments, our imaging system can detect single micron-scale particles or clouds of smaller particles. With diffusion length of the order of a few microns during the growth time, it is unlikely that large particles [Fig. 3(b)] came with the arc, but rather they formed from smaller particles. Arc motion forms nonstationary environments for nanoparticles in the plasma. These particles are subjected to time-dependent fluxes of plasma species and heat flux. Their resulting effect on nanoparticles depends on their surface-to-volume ratio and the nature of the exerted forces. In particular, the heating of nanoparticles by the arc radiation field [19] should increase with the particle surface area. Then temperature-dependent thermionic emission from nanoparticles can affect the nanoparticle charging and potential with respect to the plasma [20]. We show below that under nonstationary arc conditions, size-dependent heating of nanoparticles and resulting thermionic emission can form a bipolar charge distribution of nanoparticles causing a Coulomb attraction and continuous growth of particles.

To mimic experimental observations when particles are exposed to time-dependent charge and heat fluxes due to arc movement, we model the behavior of a group of particles with diameters greater than or equal to 10 nm placed near the arc (Fig. 1). We assume that at time $t = 0$ the arc is located close to the region of particles growth ($r_{\min}$ at ①) and reaches apogee ($r_{\max}$ at ②) in about 0.5 ms. We consider spherical nanoparticles of radii $r_{\rm np}$ at a distance from the arc $r = r_{\min} = 1$ cm with initial temperature $T_{\rm np}$ being equal to the local gas temperature $T_{\rm gas} = 1500$ K. The local plasma Debye length λ_D (about 8 μm for $n_e = 1.5 \times 10^{17}$ m^{-3} and $T_e = 2000$ K; see Fig. 2) is comparable to the mean free path $\lambda_{\rm mfp}$ of ion-neutral collisions $\sim$5 μm between carbon ions and He atoms ($p_{\rm gas} = 500$ Torr). The local density of carbon neutrals is much lower, which makes the contribution of charge-exchange collisions negligible. At these conditions, the relation $r_{\rm np} \ll \lambda_D \cong \lambda_{\rm mfp}$ holds, thus allowing us to apply a collisionless charging model, although at its very limit. We further assume the equilibrium state of plasma around nanoparticles, isotropic heating, and charging and that properties of nanoparticle material relevant to heat exchange and thermionic emission processes are identical to larger particulates. While nanoparticles do not necessarily behave in the same manner as larger particulates in the considered processes, we are not aware of experimental data or modeling results which comply with this aspect and could be applied in the current study.

The plasma electron and ion fluxes to nanoparticles together with the plasma radiation lead to the heating of nanoparticles. Thermal radiation and electron emission cause cooling of nanoparticles. Moreover, there is also a heat exchange with surrounding gas. Under dynamic equilibrium, the temperature of the particles reaches steady state when the heat fluxes to and from the particles are balanced. Since the heat exchange with the plasma is determined by the sheath potential of the nanoparticle with respect to the plasma, the steady-state potential is governed by the balance of all charge fluxes between the particles and the plasma. These heat and charge flux balances are described [21] as (see Fig. 1)

$$\begin{aligned} Mc_{\rm heat}\frac{dT_{\rm np}}{dt} &= Q_{\rm abs} + Q_{\rm pl} - Q_{\rm rad} - Q_{\rm gas} - Q_{\rm em}, \\ C_{\rm np}\frac{d\phi_{\rm np}}{dt} &= I_{\rm TE} + I_e + I_i, \end{aligned} \tag{1}$$

where M, $c_{\rm heat}$, $C_{\rm np}$, and $\phi_{\rm np}$ are the particle mass, heat capacity, capacitance, and potential with respect to plasma bulk, respectively. Here we have introduced the following parameters: (i) the heat flux from the radiating arc (Rayleigh regime $\frac{r_{\rm np}}{\lambda_{\rm arc}} \ll 1$) [19]

$$Q_{\rm abs} = K_{\rm abs}\frac{r_{\rm np}^3 T_{\rm arc}^5}{r^2},$$

where $T_{\rm arc}$ is the arc core temperature and $K_{\rm abs} = \frac{32\eta\pi^2 E_m \sigma_{\rm SB} k_B}{hc} R_{\rm arc}^2$, with $\sigma_{\rm SB} = \frac{2}{15}\frac{\pi^4 k_B^4}{h^3 c^2}$ the Stefan-Boltzmann constant, $\eta = 0.8$ the emissivity of the arc, $E_m = 0.35$ a broadband value of the complex refractive index taken as for soot particles, and $R_{\rm arc} = 2$ mm the arc core radius; (ii) the heat flux from the plasma species

$$Q_{\rm pl} = |I_i|(E_{\rm ion} - \phi_w - \phi_{\rm np}) + |I_e|(\phi_w + \phi_{\rm np}),$$

where $E_{\rm ion}$ is an ionization energy for carbon (11.26 eV) and ϕ_w is the work function of the particle material (4.7 eV), with the electron and ion currents [6]

$$I_k = \begin{cases} K_k q_k\left(1 - \frac{q_k\phi_{\rm np}}{k_B T_k}\right) & \text{if } q_k\phi_{\rm np} < 0 \\ K_k q_k \exp\left\{\frac{-q_k\phi_{\rm np}}{k_B T_k}\right\} & \text{if } q_k\phi_{\rm np} > 0, \end{cases}$$

where $k = e, i$ stands for electrons and ions, respectively, $K_k = n_k\sqrt{\frac{k_B T_k}{2\pi m_k}}$, $q_e = -e$, $q_i = e$, e is the absolute value of the electron charge, $n_e(n_i)$ and $T_e(T_i)$ are the plasma electron (carbon ion) density and temperature, respectively, m_e (m_i) is the electron (carbon ion) mass, and k_B is the Boltzmann constant; the OML approximation is applied here ($\frac{r_{\rm np}}{\lambda_D} \ll 1$ and $\frac{T_{\rm np}}{T_e} \approx 1$, where $\lambda_D = \sqrt{\frac{\epsilon_0 k_B T_e}{2e^2 n_e}}$ is the Debye length, with $T_e = T_i$); (iii) the particle radiation (in Rayleigh regime) [19]

$$Q_{\rm rad} = K_{\rm rad} r_{\rm np}^3 T_{\rm np}^5,$$

where $K_{\rm rad} = \frac{32\eta\pi^2 E_m \sigma_{\rm SB} k_B}{hc}$; (iv) the gas cooling [22]

$$Q_{\rm gas} = K_{\rm gas} r_{\rm np}^2,$$

which is calculated in a free molecular regime (Knudsen number $K_n > 1$), where $K_{\rm gas} = 2\pi\alpha_T p\sqrt{\frac{R_m}{2\pi M_{\rm He}}}\frac{\gamma+1}{\gamma-1}$, with $\alpha_T = 0.1$ a thermal accommodation coefficient for helium, p and $M_{\rm He}$ the helium pressure and molar mass, respectively, R_m a universal gas constant, and $\gamma = 5/3$ the specific heat ratio; and (v) cooling due to thermionic emission, where we neglect secondary electron emission, photoemission, and field emission as they are nondominant in the arc as compared to thermionic emission; under such conditions, the cooling is given by

$$Q_{\rm em} = I_{\rm TE}(\phi_w + \phi_{\rm np} + 2k_B T_{\rm np}),$$

where $I_{\rm TE}$ is the Richardson-Dushman thermoemission current

$$I_{\rm TE} = \begin{cases} K_{\rm TE}\exp\left\{\frac{-e(\phi_w - \delta\phi)}{k_B T_{\rm np}}\right\}, & \phi_{\rm np} < 0 \\ K_{\rm TE}\left(1 + \frac{e\phi_{\rm np}}{k_B T_{\rm np}}\right)\exp\left\{\frac{-e(\phi_w + \phi_{\rm np})}{k_B T_{\rm np}}\right\}, & \phi_{\rm np} > 0, \end{cases}$$

where an exponential term with $\delta\phi = \sqrt{\frac{-e\phi_{\rm np}}{4\pi\epsilon_0 r_{\rm np}}}$ accounts for the Schottky effect [19] and $K_{\rm TE} = \frac{4\pi e m_e k_B^2}{h^3} r_{\rm np}^2 T_{\rm np}^2$.

Figure 4 show the time evolution of temperature and the potential for considered particles by solving Eqs. (1) simultaneously. Our model predicts that for all considered sizes, the nanoparticles reach their steady-state temperatures in 10–50 μs [Fig. 4(a)]. The time to reach the equilibrium state increases with the particle size. For example, a 50-nm particle reaches a steady-state temperature of about 3000 K in 20 μs. At this temperature, particle mass losses due to sublimation become appreciable (approximately equal to 3%). For smaller particles, the temperature is lower and as a result the mass loss due to sublimation is estimated to be negligible (less than 1%). When the particle temperature is below 2000 K, the particle charge is governed by the fluxes of ions and electrons from the plasma. This is because the thermionic emission is insignificant at such low temperatures. As a result, the flux of electrons emitted from the particle is negligible as compared to the flux of plasma electrons to this particle. Under such conditions, the potential of the particle with respect to the plasma is at

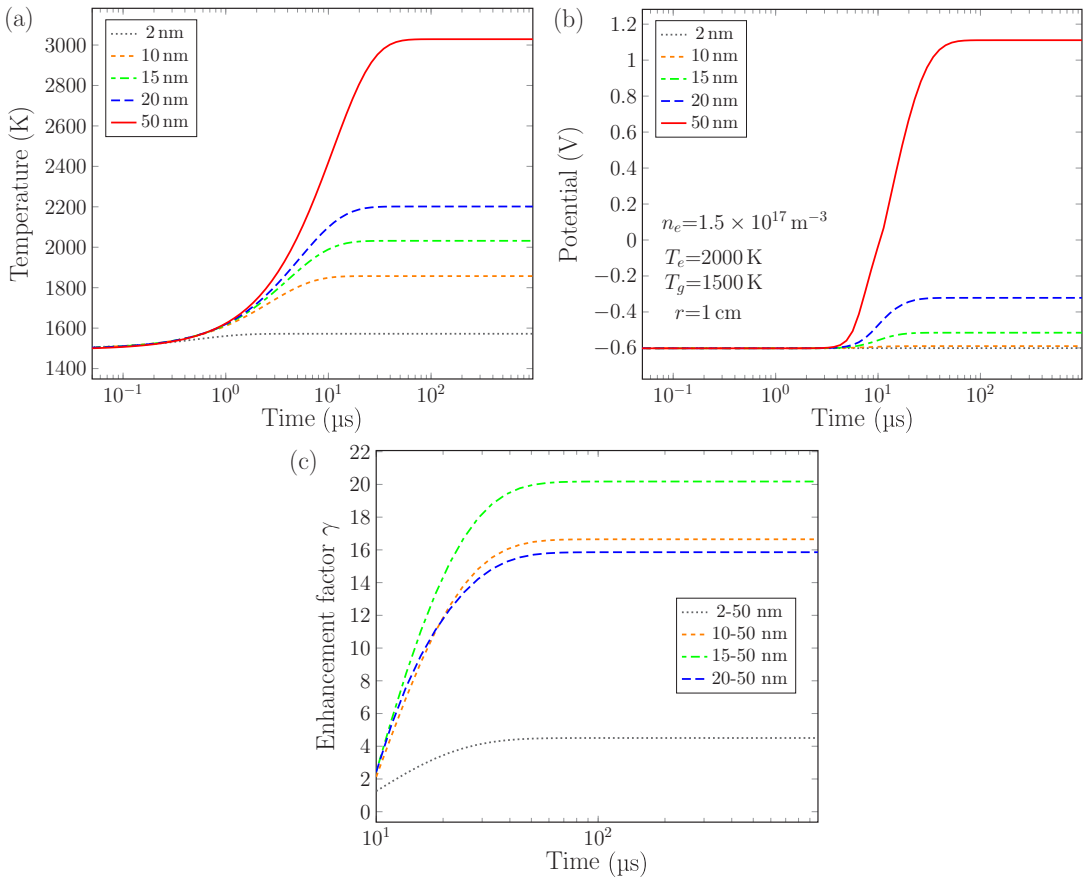

FIG. 4. Time evolution of (a) temperature and (b) potential of particles and (c) enhancement factor γ between selected pairs of particles closest to the arc distance. Model parameters (electron density n_e, temperature T_e, gas temperature T_{gas}, and distance to the arc $r = r_{\text{min}}$) used in modeling are shown in (b).

its minimum (i.e., the maximum potential difference between particle and the plasma). For the particles considered here, the minimum potential stays for a few microseconds [Fig. 4(b)]. Further in time, the particle temperature increases due to arc radiation absorption and saturates, balancing the terms on the right-hand side of Eq. (1). As a result, the thermionic emission flux increases and, depending on the particle size, can become comparable to the flux of plasma electrons or even exceed it. This process leads to a decrease of the potential difference between the nanoparticle and bulk plasma as well as the number of trapped ions [9] which can substantially affect the potential distribution near the nanoparticle. In this case the sheath potential distribution is mostly determined by electrons thermionically emitted from the hot nanoparticle, whereas the role of trapped ions is secondary. A loss of electrons by thermionic emission coupled with undercompensated net incoming negative charge flux triggers the growth of a nanoparticle positive charge. At some moment this process equals the nanoparticle potential with the plasma potential and further makes it positive relative to the plasma. Here the potential of the nanoparticle is defined with respect to the plasma potential in the vicinity of the nanoparticle (sheath size). Having a positive potential with respect to the local plasma potential implies that the net charge of the nanoparticle is positive with respect to the space potential. This is assuming that the sheath potential changes monotonically between the nanoparticle and the plasma or any nonmonotonic changes are insignificant as compared to the total potential drop in the plasma-nanoparticle sheath. In the model, the flux of charged particles (ions and electrons) is self-consistently calculated as a function of the nanoparticle potential (relative to the plasma potential) during the simulation time domain to account for these effects and carefully track the polarity change.

This process results in the formation of a bipolar size distribution of particles. In particular, for the considered conditions, there is a particle-size threshold (∼40 nm) below which particles are negatively charged and above which particles are positively charged. This size-charge distribution is a reversal of the distribution derived in Ref. [8] for a low-pressure capacitively coupled rf plasma due to a difference in charging mechanism.

The formation of this bipolar charge distribution of particles enhances the coagulation process due to attractive Coulomb interaction. Without external forces the Brownian coagulation rate β between neutral particles of radii r_i and r_j was derived by Smoluchowski. In a free molecular regime ($K_n > 1$) the coagulation rate is

$$\beta(r_i, r_j) = \left(\frac{3}{4\pi}\right)^{1/6} (r_i + r_j)^2 \sqrt{\frac{6k_B}{\rho}\left(\frac{T_i}{r_i^3} + \frac{T_j}{r_j^3}\right)}, \qquad (2)$$

where ρ is the particle density and T is the particle temperature. The effects of van der Waals forces, thermophoresis, and acoustic and electrostatic fields are commonly accounted for via correction coefficients for the coagulation rates. Following the work of Fuchs [23], the rate coefficient in the case of bipolar charging of particles is enhanced by a factor

$$\gamma = \frac{1 - e^{-\lambda}}{\lambda}, \quad \lambda = \frac{-|q_i q_j|}{2\pi\epsilon_0(r_i + r_j)k_B(T_i + T_j)}, \qquad (3)$$

which we further refer to as an enhancement factor; it is plotted in Fig. 4(c).

IV. DISCUSSION

Our model shows that particles exposed to the arc radiation are subjected to bipolar charging which promotes growth rates exceeding those between neutral particles. Furthermore, the growth of big micron-size particles observed in experiment is not suppressed by the Coulomb repulsion forces. The typical response time of particles to the variation of external conditions is about 100 μs (see Fig. 4) and the threshold particle size at which the charge reversal happens is sensitive to the arc distancing. It is shown that favorable conditions for continuous growth of particles are naturally formed in an oscillating arc (with frequencies in the kilohertz range) as supported by observation (Fig. 3). It is important to emphasize that an oscillating arc affecting particles manifests itself in a sporadic motion of the arc core between the arc electrodes. This motion is also a source of acoustic perturbations in the surrounding weakly ionized plasma [18,24]. As shown in Refs. [25,26], the larger particles with a size larger than the mean free path of gas atoms or molecules ($K_n < 1$) can be rapidly fused in the acoustic field to micrometer-size aggregates, as observed in experiment. At some point, the aggregated particles become heavy enough to fall away from the growth region. This mass-separation process may limit the maximum size of particles grown in the arc. A self-consistent modeling of particle coagulation in a dynamic plasma is needed to extend this work to other laboratory and space plasmas.

V. CONCLUSION

In summary, submillisecond growth times of micron-scale particles were observed in an oscillating carbon arc at subatmospheric pressure. This experimental observation was modeled by accounting for time-dependent fluxes of energy and charges from plasma to the nanoparticles. Our model predicts the formation of a bipolar charge distribution of nanoparticles leading to the enhanced coagulation rates between oppositely charged nanoparticles. In particular, the formation of a bipolar charge distribution is mainly governed by the interplay between arc-induced radiative heating of the nanoparticles and cooling of these nanoparticles by thermionic electron emission. In addition to arcs, this interplay can also be implemented in dusty plasmas with external heating of particles by, for example, lasers or infrared lamps and in plasmas generated by laser vaporization of solid targets. Among the practical applications of plasmas with a controllable bipolar distribution of particles is assembling and manufacturing of three-dimensional structures in plasma volume.

ACKNOWLEDGMENTS

The authors are grateful to A. Merzhevsky for support with assembly of the experimental setup and to Dr. A. Khrabry, Dr. S. Yatom, Dr. I. Kaganovich, and Dr. B. Stratton for fruitful discussions. This work was supported by the U.S. Department of Energy, Office of Science, Basic Energy Sciences, Materials Sciences and Engineering Division.

[1] A. P. Nefedov, O. F. Petrov, and V. E. Fortov, Phys. Usp. **40**, 1163 (1997).
[2] A. V. Filippov, A. F. Pal', and A. N. Starostin, J. Exp. Theor. Phys. **121**, 909 (2015).
[3] M. Horanyi and C. Goertz, Astrophys. J. **361**, 155 (1990).
[4] M. Shiratani, H. Kawasaki, T. Fukuzawa, T. Yoshioka, Y. Ueda, S. Singh, and Y. Watanabe, J. Appl. Phys. **79**, 104 (1996).
[5] J. Goree, Plasma Sources Sci. Technol. **3**, 400 (1994).
[6] E. C. Whipple, Rep. Prog. Phys. **44**, 1197 (1981).
[7] D. S. Lemons, R. K. Keinigs, D. Winske, and M. E. Jones, Appl. Phys. Lett. **68**, 613 (1996).
[8] L. Ravi and S. L. Girshick, Phys. Rev. E **79**, 026408 (2009).
[9] J. Goree, Phys. Rev. Lett. **69**, 277 (1992).
[10] H. M. Mott-Smith and I. Langmuir, Phys. Rev. **28**, 727 (1926).
[11] G. L. Delzanno and X.-Z. Tang, Phys. Rev. Lett. **113**, 035002 (2014).
[12] V. Vekselman, M. Feurer, T. Huang, B. Stratton, and Y. Raitses, Plasma Sources Sci. Technol. **26**, 065019 (2017).
[13] V. Vekselman, A. Khrabry, I. Kaganovich, B. Stratton, R. S. Selinsky, and Y. Raitses, Plasma Sources Sci. Technol. **27**, 025008 (2018).
[14] S. Yatom, J. Bak, A. Khrabryi, and Y. Raitses, Carbon **117**, 154 (2017).
[15] P. K. Shukla and B. Eliasson, Rev. Mod. Phys. **81**, 25 (2009).
[16] See Supplemental Material at http://link.aps.org/supplemental/10.1103/PhysRevE.99.063205 for the recorded video file of particle growth in the carbon arc.
[17] F. Liang, M. Tanaka, S. Choi, and T. Watanabe, J. Phys.: Conf. Ser. **518**, 012027 (2014).
[18] S. Gershman and Y. Raitses, J. Phys. D **49**, 345201 (2016).
[19] M. N. Shneider, Phys. Plasmas **22**, 073303 (2015).
[20] G. L. Delzanno, G. Lapenta, and M. Rosenberg, Phys. Rev. Lett. **92**, 035002 (2004).
[21] J. M. Mitrani, M. N. Shneider, B. C. Stratton, and Y. Raitses, Appl. Phys. Lett. **108**, 054101 (2016).
[22] A. Filippov and D. Rosner, Int. J. Heat Mass Transf. **43**, 127 (2000).
[23] N. Fuchs, Z. Phys. **89**, 736 (1934).
[24] F. K. Popov and M. N. Shneider, J. Appl. Phys. **122**, 053303 (2017).
[25] M. N. Shneider, *Proceedings of the 54th AIAA Aerospace Sciences Meeting, San Diego, 2016* (American Institute of Aeronautics and Astronautics, Reston, 2016), p. 14266.
[26] S. Yatom, A. Khrabry, J. Mitrani, A. Khodak, I. Kaganovich, V. Vekselman, B. Stratton, and Y. Raitses, MRS Commun. **8**, 842 (2018).